Asociación Argentina
de Mecánica Computacional

Mecánica Computacional Vol XXIX, págs. 4585-4599 (artículo completo)
Eduardo Dvorkin, Marcela Goldschmit, Mario Storti (Eds.)
Buenos Aires, Argentina, 15-18 Noviembre 2010

NUMERICAL MODELS FOR THE THREE DIMENSIONAL ANALYSIS OF THE ACOUSTIC BEHAVIOUR INSIDE A PARALELIPIPEDIC SPACE

Edmundo G. de A. Costa[a], Luís M. C. Godinho[b], Andreia S. C. Pereira[b] and José A. F. Santiago[a]

[a]*COPPE/Federal University of Rio de Janeiro, Department of Civil Engineering, Caixa Postal 68506, CEP 21945-972, Rio de Janeiro, RJ, Brazil, edmundo_costa@coc.ufrj.br, santiago@coc.ufrj.br, http://www.coc.ufrj.br/*

[b]*CICC, Department of Civil Engineering, University of Coimbra, Pinhal de Marrocos, 3030-788, Coimbra, Portugal, lgodinho@dec.uc.pt, apereira@dec.uc.pt, http://www.dec.uc.pt*

Keywords: Boundary Element Method, Method of Fundamental Solutions, Confined Spaces, Green's functions.

Abstract. In the present work, numerical frequency domain formulations are developed for the prediction of the acoustic behavior inside a three dimensional perfectly rigid enclosure in the presence of a point source. In these formulations the Boundary Element Method (BEM) and the Method of Fundamental Solutions (MFS) are used with appropriate Green's functions that allow to reduce the number of discretized surfaces. The aim here is to find numerical strategies that may allow to reduce computational cost and improve accuracy. These models will further permit for an analysis in higher frequencies as less computer resources are required due to reduced discretization. The possibility of assigning different absorption properties to the interfaces and of assuming different room shapes by inclining some of the interfaces is also here addressed.
A detailed analysis on the behavior of the models for different cases is performed highlighting accuracy, efficiency and stability of the numerical strategies here proposed. Simulations are displayed for the simple case of a small room where low frequency domain responses regarding sound pressure level have been computed and the results obtained are compared with experimental results.

1 INTRODUCTION

During the last three decades, the Boundary Element Method (BEM) has established itself as one of the preferred methods to be used for acoustics and vibro-acoustics engineering analysis. In fact, the BEM has a number of advantages over other numerical methods that contribute to its success (Brebbia (1984)): (i) it only requires the discretization of the problem boundaries, and thus only involves a more compact description of the environment; (ii) it has a very good accuracy, since it is based on the use of Green's functions, which are, themselves, a solution of the governing equation; (iii) it is very well suited to the analysis of infinite or semi-infinite domains, as the far-field radiation conditions are automatically satisfied. Some of these advantages are even more pronounced when a 3D analysis in an infinite/semi-infinite domain is considered, for which alternative methods frequently require millions of degrees of freedom, together with a truncation of the propagation domain and the use of approximate absorbing boundary conditions.

Through the years, many researchers have used the method in acoustic analysis of different systems. Many resources for the BEM can be found, such as the excellent book by Wu, (2000), which describes the principles of the boundary element method for acoustic analysis. Interesting developments can be found in many scientific papers, such as the early works of Lacerda et al. (1997), in which a dual BEM formulation is used to analyze the 2D sound propagation around acoustic barriers, over an infinite plane, considering both the ground and the barrier to be absorptive. Later, the 3D propagation of sound around an absorptive barrier has been studied by the same authors (Lacerda et al. (1998)), introducing a dual boundary element formulation that allowed the barrier to be modeled as a simple surface.

An interesting feature of the BEM is that it can be adapted to include more complex Green's functions, accounting for the presence of specific features of the propagation medium. It is the case of the works of Godinho et al. (2001) and Tadeu et al. (2007), analyzing the specific case of 2D configurations subject to the effect of a 3D pressure source, using the BEM to study the effect of acoustic barriers and of thin screens coupled to a building façade in the reduction of traffic noise. In those studies, both the rigid ground and the rigid façade are taken into account by using the image-source method, thus avoiding their discretization. Additionally, those authors synthesize the 3D sound field as a summation of simpler 2D problems (also known as a 2.5D formulation), with much lower computational cost.

In the last years, several researchers have been focusing their attention on another class of methods, the meshless methods, with the goal of reducing computation time and the time consuming task of mesh generation that complex geometries require. The Method of Fundamental Solution is one of these methods that have been applied with success to solve acoustic problems. The mathematical formulation of MFS is quite simple requiring the knowledge of fundamental solutions. Fairweather et al. (2003) described and reviewed the MFS and related methods for the numerical solution of scattering and radiation problems in fluids and solids. Alves and Valtchev (2005) compared the plane waves method and the MFS for acoustic wave scattering. Chen et al. (2002) employed the boundary collocation method using radial basis functions for the acoustic eigen-analysis of three-dimensional (3D) cavities.

In this work the three dimensional sound field generated by a point source placed inside a parallelepipedic space is here analyzed using frequency domain formulations based on the Boundary Element Method and on the Method of Fundamental Solution. The models here developed make use of adequate Green's functions therefore requiring the discretization of a limited number of surfaces. The main objective of this paper is to analyze the advantages of incorporating these functions in models based on these methods. The possibility of assigning

absorption properties and assuming inclined interfaces is here discussed. The behavior of the numerical approaches is discussed by analyzing stability, accuracy and efficiency. Finally an application is displayed where frequency domain responses are computed for a room and compared with experimental results.

2 PROBLEM FORMULATION

The propagation of sound within a three-dimensional space can be mathematically given in the frequency domain by the Helmholtz partial differential equation,

$$\nabla^2 p + k^2 p = -\sum_{k=1}^{NS} Q_k \delta(\xi_k^f, \xi), \tag{1}$$

where $\nabla^2 = \frac{\partial^2}{\partial x^2} + \frac{\partial^2}{\partial y^2} + \frac{\partial^2}{\partial z^2}$; p is the acoustic pressure, $k = \omega/\alpha$; $\omega = 2\pi f$; f is the frequency; α is the sound propagation velocity within the acoustic medium; *NS* is the number of sources in the domain; Q_k is the magnitude of the existing sources ξ_k^f located at $(x_{\xi_k^f}, y_{\xi_k^f})$; ξ is a domain point located at (x_ξ, y_ξ) and $\delta(\xi_k^f, \xi)$ is the Dirac delta generalized function.

The boundary conditions for the problem are given by:

$$v_n(\mathbf{x}) = \frac{\partial p}{\partial \mathrm{n}}(\mathbf{x}) = 0 \qquad \text{in interfaces } S_v \tag{2a}$$

$$p(\mathbf{x}) = Z(\mathbf{x}) v_n(\mathbf{x}) \qquad \text{in interfaces } S_Z \tag{2b}$$

where $Z(\mathbf{x})$ is the surface impedance of the absorbing material, which is assumed to be a known quantity. Equation (2a) stands for Neumann condition and equation (2b) stands for Robin or mixed boundary condition.

Considering that a point source is placed within this propagation domain, at $\boldsymbol{x}_0$, it is possible to establish the fundamental solution for the sound pressure at a point $\boldsymbol{x}$, which can be written as

$$G(\xi, \mathbf{x}) = \frac{\mathrm{e}^{-\mathrm{i}kr}}{4\pi r}, \text{ with } \quad r = \sqrt{(x-x_0)^2 + (y-y_0)^2 + (z-z_0)^2}\,. \tag{3}$$

3 NUMERICAL FORMULATION

3.1 BEM Formulation

According to Green's Second Identity, Eq. (1) can be transformed into the following boundary integral equation:

$$C(\xi) p(\xi) = -\mathrm{i}\rho\omega \int_S G(\xi, \mathbf{x}) v_n(\mathbf{x}) \mathrm{d}S - \int_S \frac{\partial G(\xi, \mathbf{x})}{\partial n} p(\mathbf{x}) \mathrm{d}S + \sum_{k=1}^{NS} Q_k G(\xi_k^f, \xi), \tag{4}$$

where $S = S_v \cup S_Z$ refers to the discretized interfaces and $G(\xi, \mathbf{x})$ is the fundamental solution; $p(\mathbf{x})$ and $v_n(\mathbf{x})$ represent the acoustic pressure and the normal derivative of the acoustic pressure, respectively. The coefficient $C(\xi)$ depends on the boundary geometry at the source

point.

In order to solve Equation (4), the Boundary Element Method may be used, requiring discretization of all surfaces, if appropriate fundamental solutions are not employed. Here, the previously described wave propagation problem using the BEM is solved using two different Green's functions that satisfy specific boundary conditions allowing for reduction of boundary discretization. Two BEM models are defined: the first one makes use of a fundamental solutions valid for a space defined by three orthogonal planes, therefore three surfaces need to be discretized (BEM - Model 1, as displayed in Figure 1a); the second BEM model (BEM - Model 2, displayed in Figure 1b) makes use of a fundamental solution valid for a space defined by five orthogonal planes, therefore only one interface is discretized. Details on these functions will be given in a subsequent section.

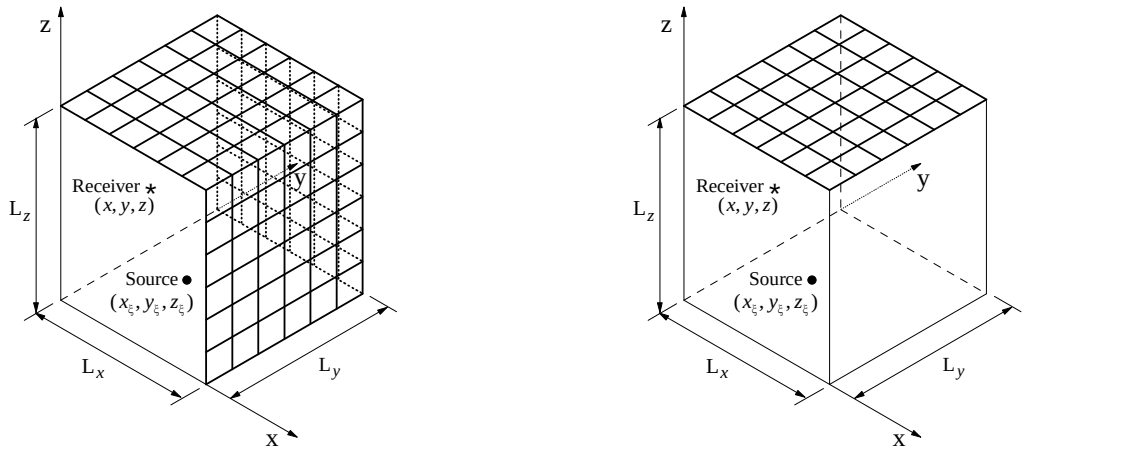

Figure 1: Geometry of the BEM models: a) BEM - Model 1; b) BEM - Model 2.

Since the appropriate Green's function are used, introducing Equations (2) into Equation (4) and assuming NE_B constant elements with linear geometry at the discretized interfaces, by applying the collocation method to the integral equation, in terms of an intrinsic coordinate η, the following equations can be obtained:

$$C(\boldsymbol{\xi}_p)\,p(\boldsymbol{\xi}_p) = -\sum_{q=1}^{NE_B}\int_{-1}^{1}\int_{-1}^{1}\frac{\partial G(\boldsymbol{\xi}_p,\mathbf{x}_q)}{\partial n}p(\mathbf{x}_q)\left|J\right|\mathrm{d}\eta_1\mathrm{d}\eta_2 + \sum_{k=1}^{NS}Q_k G(\boldsymbol{\xi}_k^f,\boldsymbol{\xi}_p), \tag{5a}$$

$$\begin{aligned} C(\boldsymbol{\xi}_p)\,p(\boldsymbol{\xi}_p) = {} & -\mathrm{i}\rho\omega\sum_{q=1}^{NE_B}\int_{-1}^{1}\int_{-1}^{1}G(\boldsymbol{\xi}_p,\mathbf{x}_q)p(\mathbf{x}_q)/Z(\mathbf{x}_q)\left|J\right|\mathrm{d}\eta_1\mathrm{d}\eta_2 - \\ & \sum_{q=1}^{NE_B}\int_{-1}^{1}\int_{-1}^{1}\frac{\partial G(\boldsymbol{\xi}_p,\mathbf{x}_q)}{\partial n}p(\mathbf{x}_q)\left|J\right|\mathrm{d}\eta_1\mathrm{d}\eta_2 + \sum_{k=1}^{NS}Q_k G(\boldsymbol{\xi}_k^f,\boldsymbol{\xi}_p), \end{aligned} \tag{5b}$$

where $\boldsymbol{\xi}_p$ refers to the functional node p with p ranging from 1 to NE_B; $\left|J\right|$ is the Jacobian, $p(\mathbf{x}_q)$ is the unknown acoustic pressure at the boundary element $\mathbf{x}_q$; $G(\boldsymbol{\xi}_p,\mathbf{x}_q)$ refers to the fundamental solution whose details will be given in a subsequent section; $G(\boldsymbol{\xi}_k^f,\boldsymbol{\xi}_p)$ is the incident field regarding the pressure generated by the real source k placed at position $\boldsymbol{\xi}_k^f$. Equation (5a) is applied if the discretized surfaces are perfectly rigid, whereas equation (5b) is

employed if assigning absorption to the discretized surfaces. For both cases we obtain a system of $NE_B \times NE_B$ equations, which after solving it makes it possible to obtain the acoustic pressure at any point of the domain by applying the boundary integral equation.

3.2 MFS formulation

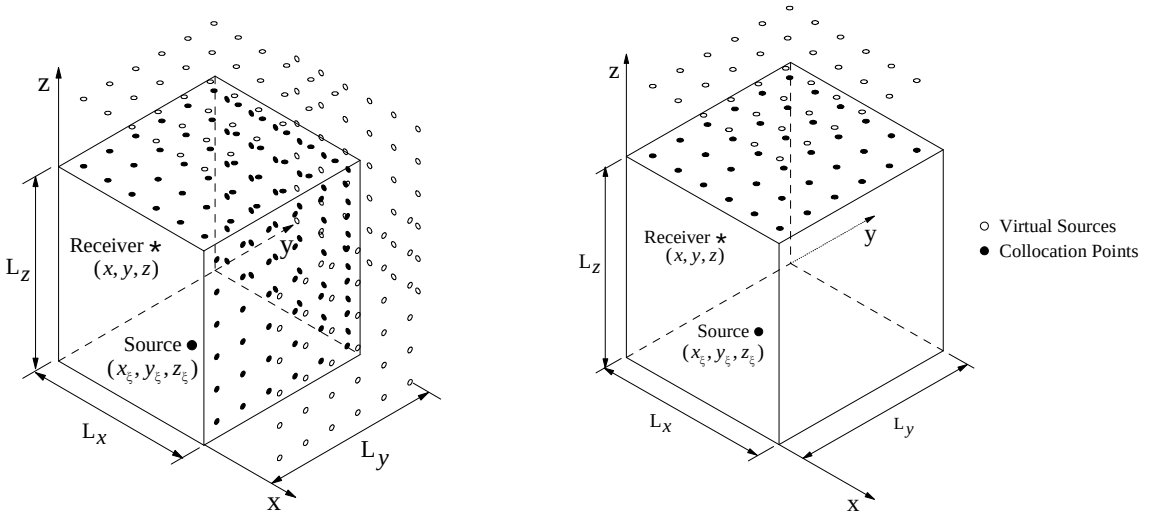

Figure 2: Geometry of the MFS models: a) MFS - Model 1; b) MFS - Model 2.

Using the Method of Fundamental Solutions the frequency domain response inside a three dimensional enclosure is computed as a linear combination of fundamental solutions for a set of NVS virtual sources, with amplitude A_l (with $l = 1,...,NVS$), placed outside the domain of interest, to avoid singularities. Thus, the pressure field inside the parallelepipedic space is given by,

$$p(\xi, \mathbf{x}) = \sum_{l=1}^{NVS} A_l G\left(\xi_l, \mathbf{x}\right) + \frac{e^{-ik\sqrt{(x-x_0)^2+(y-y_0)^2+(z-z_0)^2}}}{4\pi\sqrt{(x-x_0)^2+(y-y_0)^2+(z-z_0)^2}}, \tag{6}$$

where the coefficients A_l are unknown amplitudes which are computed by imposing the appropriate boundary conditions at a set of NCP points (collocation points) placed along the virtual interfaces $S = S_\upsilon \cup S_Z$ and $G\left(\xi_l, \mathbf{x}\right)$ is the fundamental solution at point $\mathbf{x}$ for a virtual source ξ_l. In this work an equal number of collocation points and virtual sources are assumed which allows to obtain a NVS x NVS system. This system is built by prescribing at the virtual boundaries of the parallelepiped space the following conditions: expression (2a), if the virtual discretized interfaces are assumed perfectly rigid or expression (2b) if assigning absorption to the virtual discretized interfaces. Here again two models were developed: in the first model (MFS – Model 1) only three virtual interfaces need to be assumed, whereas in the second model only a virtual interface needs to be considered (MFS – Model 2), as displayed in Figure 2.

3.3 Green's functions

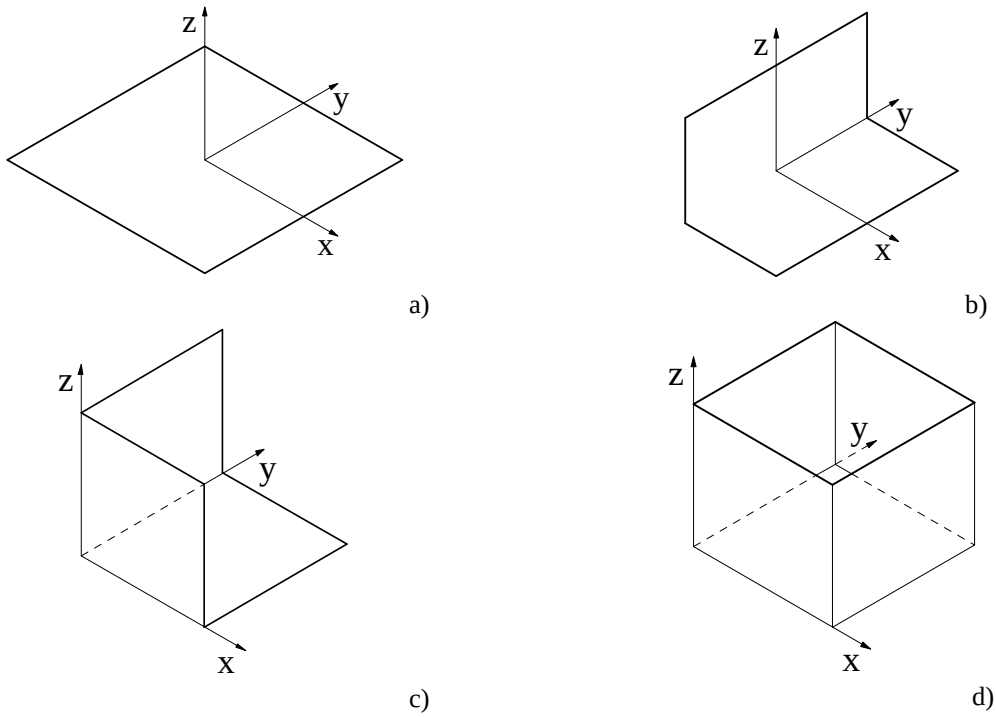

Figure 3: Geometry of the Green's functions: a) Half-space; b) Quarter space; c) 3 surfaces; d) 5 surfaces.

In an acoustic analysis, the presence of perfectly reflecting plane surfaces can be taken into account by using the well-known image-source method. In this technique, the effect of a point source in the presence of a given plane surface can be simulated by considering an additional virtual source, positioned in a symmetrical position with respect to the reflecting plane. Thus, following, for example, Godinho et al. (2001), if such plane is defined by $z = 0$ (see Figure 3a), the corresponding Green's function can be written as

$$G_{1S}(\boldsymbol{\xi}, \mathbf{x}) = \frac{\mathrm{e}^{-\mathrm{i}kr}}{4\pi r} + \frac{\mathrm{e}^{-\mathrm{i}kr_1}}{4\pi r_1}, \text{ with } r_1 = \sqrt{(x - x_0)^2 + (y - y_0)^2 + (z + z_0)^2}\,. \tag{7}$$

This approach can be further extended to incorporate more surfaces. Considering, for example, a "quarter-space" defined by two orthogonal planes, one located at $z = 0$ and the other at $x = 0$ (see Figure 3b), the corresponding Green's function can be written as

$$G_{2S}(\boldsymbol{\xi}, \mathbf{x}) = \frac{\mathrm{e}^{-\mathrm{i}kr}}{4\pi r} + \frac{\mathrm{e}^{-\mathrm{i}kr_1}}{4\pi r_1} + \frac{\mathrm{e}^{-\mathrm{i}kr_2}}{4\pi r_2} + \frac{\mathrm{e}^{-\mathrm{i}kr_3}}{4\pi r_3}, \tag{8}$$

with $r_2 = \sqrt{(x + x_0)^2 + (y - y_0)^2 + (z - z_0)^2}$; $r_3 = \sqrt{(x + x_0)^2 + (y - y_0)^2 + (z + z_0)^2}$.

Following the described procedure, if we consider a space defined by two vertical orthogonal planes and a horizontal plane, all perfectly rigid, placed at $x = 0$, $y = 0$ and $z = 0$, respectively, as displayed in Figure 3c, the corresponding Green's function can be expressed as:

$$G_{3S}(\boldsymbol{\xi}, \mathbf{x}) = \frac{e^{-\mathrm{i}kr}}{4\pi r} + \sum_{i=1}^{7} \frac{e^{-\mathrm{i}kr_i}}{4\pi r_i}, \tag{9}$$

with $r_4 = \sqrt{(x-x_0)^2+(y+y_0)^2+(z+z_0)^2}$; $r_5 = \sqrt{(x-x_0)^2+(y+y_0)^2+(z-z_0)^2}$; $r_6 = \sqrt{(x+x_0)^2+(y+y_0)^2+(z-z_0)^2}$ and $r_7 = \sqrt{(x+x_0)^2+(y+y_0)^2+(z+z_0)^2}$.

If we assume a space defined by five planes four vertical orthogonal planes ($x=0$, $x=L_x$, $y=0$, $y=L_y$) and one horizontal plane, placed at $z=0$, as defined in Figure 3d, the corresponding Green's function can be expressed as:

$$G_{5S}(\boldsymbol{\xi},\mathbf{x}) = \frac{e^{-\mathrm{i}kr_{000}}}{4\pi r_{000}} + \sum_{n=0}^{NSY}\left(\sum_{j=1}^{4}\frac{e^{-\mathrm{i}kr_{0j0}}}{4\pi r_{0j0}}\right) + \sum_{m=0}^{NSX}\sum_{i=1}^{4}\left[\frac{e^{-\mathrm{i}kr_{i00}}}{4\pi r_{i00}} + \sum_{n=0}^{NSY}\left(\sum_{j=1}^{4}\frac{e^{-\mathrm{i}kr_{ij0}}}{4\pi r_{ij0}}\right)\right] + \frac{e^{-\mathrm{i}kr_{001}}}{4\pi r_{001}} + \sum_{n=0}^{NSY}\left(\sum_{j=1}^{4}\frac{e^{-\mathrm{i}kr_{0j1}}}{4\pi r_{0j1}}\right) + \sum_{m=0}^{NSX}\sum_{i=1}^{4}\left[\frac{e^{-\mathrm{i}kr_{i01}}}{4\pi r_{i01}} + \sum_{n=0}^{NSY}\left(\sum_{j=1}^{4}\frac{e^{-\mathrm{i}kr_{ij1}}}{4\pi r_{ij1}}\right)\right], \tag{10}$$

where NSX and NSY represent the number of sources used in the x and y directions respectively, for the correct definition of the signal, and $r_{i,j,0} = \sqrt{(\underline{x}_i)^2+(\underline{y}_j)^2+(\underline{z}_0)^2}$, $r_{i,j,1} = \sqrt{(\underline{x}_i)^2+(\underline{y}_j)^2+(\underline{z}_1)^2}$ with $\underline{x}_0 = (x-x_0)$, $\underline{y}_0 = (y-y_0)$; $\underline{z}_0 = (z-z_0)$; $\underline{x}_1 = (x+x_0+2L_x m)$; $\underline{y}_1 = (y+y_0+2L_y n)$; $\underline{z}_1 = (z+z_0)$; $\underline{x}_2 = (x-2L_x-x_0-2L_x m)$; $\underline{y}_2 = (y-2L_y-y_0-2L_y n)$; $\underline{x}_3 = (x+2L_x-x_0+2L_x m)$; $\underline{y}_3 = (y+2L_y-y_0+2L_y n)$; $\underline{x}_4 = (x-2L_x+x_0-2L_x m)$; $\underline{y}_4 = (y-2L_y+y_0-2L_y n)$.

The above defined functions can be incorporated within numerical methods to avoid the full discretization of the simulated surfaces, and thus considerably reducing the computational cost of such methods.

4 BEHAVIOUR OF THE BEM AND MFS MODELS

In order to verify the proposed BEM and MFS models, consider a parallelepipedic space, with dimensions of $L_x = 1.3$ m, $L_y = 1.4$ m and $L_z = 1.5$ m, filled with air, with a density of 1.22 kg/m^3 and allowing a sound propagation velocity of 340 m/s. Consider that all the surfaces of this space are rigid, with null normal particle velocities, and that within the space a point source is located, at (x, y, z)=(0.9m, 1.0m, 0.5m), oscillating with an angular frequency $\omega = 2\pi f$.

For the above defined configuration, it becomes possible to establish an analytical solution in the form of an infinite series of image sources, reproducing the reflections at the various walls of the space. A detailed description of this solution can be found in António et al. (2008). It is important to note that, in theory, the number of sources required to reproduce the sound field in such a closed space tends to be very high, and thus the series converges slowly to the correct solution. However, the convergence of the series is greatly improved if a damped system is considered, making use of complex frequencies of the form $\omega_c = \omega - \mathrm{i}\xi\Delta\omega$, where ξ is a damping coefficient and $\Delta\omega = 2\pi\Delta f$, with Δf being the frequency step. With the aim of verifying the proposed method, this frequency increment and the damping factor were fixed at 4 Hz and $\xi = 0.7$, respectively. Those values allow just considering image sources within a distance of $1/4\ \mathrm{Hz} \times 340\ \mathrm{m/s} = 85$ m from the analyzed domain, since

sources placed further away are greatly damped and will not influence the response significantly.

The same configuration was modeled using the 3D BEM and MFS models described in the previous section. The number of boundary elements was obtained through a relation (R) between the incident wavelength and the size of the boundary, which is previously fixed. As for the MFS a similar relation between the incident wavelength and the distance between collocation points was adopted. Besides, the distance between fictitious sources and the interface was set by defining a relation (D) between this distance and the distance between collocation points.

Figure 4a illustrates the pressure computed at a receiver located at (x, y, z) = (0.4m, 0.4m, 0.5m), for frequencies between 100 Hz and 300 Hz, using the analytical solution, BEM - Model 1 assuming a relation R=15 and BEM - Model 2 with a relation R=5. In this plot, it is clear that the agreement between the analytical and the BEM solutions is excellent, and that the method was properly implemented. As for the MFS solutions, Figure 4b displays a similar response using MFS - Model 1 with R=12 and D=5 and MFS - Model 2 with R=2 and D=1.5 and the analytical solutions. Analysis of this plot confirms a good agreement among curves. These responses allows further conclusion that when using the approach where the three surfaces need to be discretized (corresponding to BEM and MFS model 1) more elements/ fictitious sources need to be assumed, in order to obtain an accurate response. Moreover when using the MFS models a lower relation R (in relation to the BEM models), may be assumed.

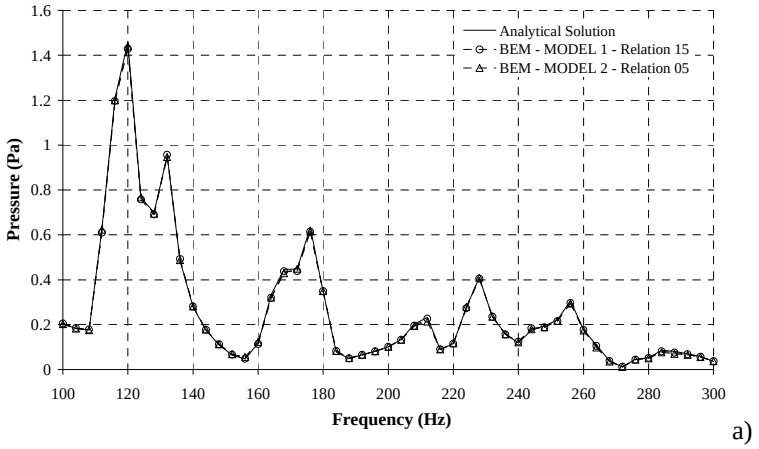

Figure 4: Pressure response obtained using the analytical solution and: a) BEM – Model 1 and BEM - Model 2; b) MFS – Model 1 and MFS – Model 2.

One of the advantages of these models in relation to analytical solutions is to have the possibility of computing the responses for a broader range of configurations. The models were therefore used to calculate the response for a similar configuration but assuming that the top surface has an inclination of 4.08º performed by increasing the size of the interface placed at $x = 0$ m to $L_z = 1.6$ m. Figure 5 displays the responses for the receiver position (0.4m, 0.4m, 0.5m). Analysis of these plots reveals good agreement among curves.

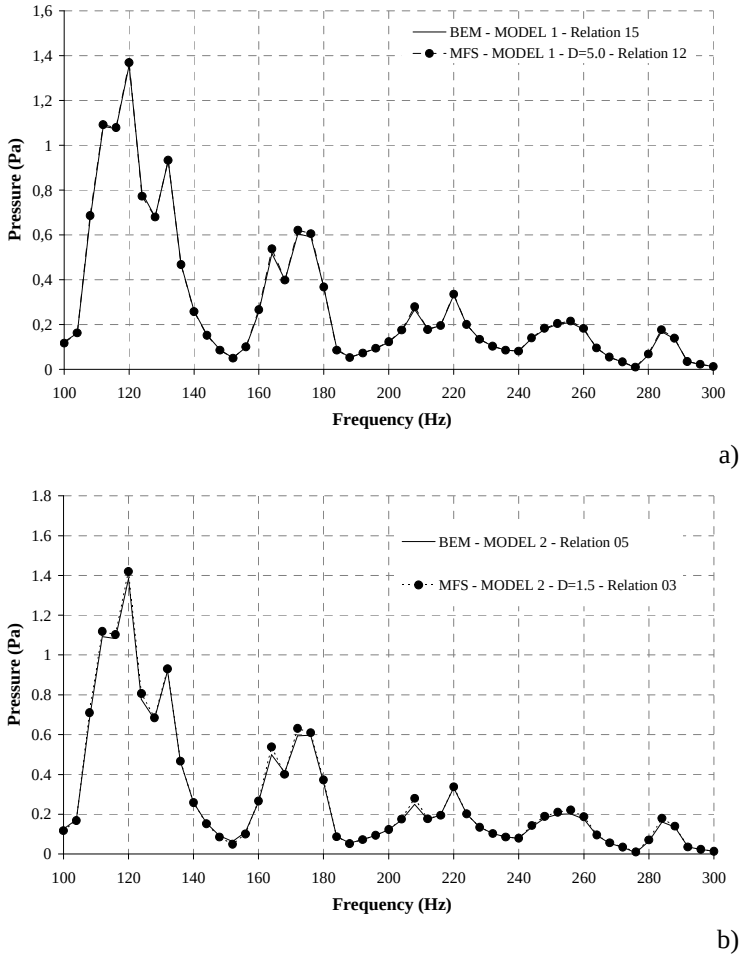

Figure 5: Pressure response obtained assuming the discretized top interface with a 4.08 º inclination using: a) BEM – Model 1 and MFS Model 1; b) BEM – Model 2 and MFS Model 2.

As mentioned in the previous section, the models allow to incorporate absorption to a discretized interface by defining the surface impedance of the absorbing material, which is assumed to be a known quantity. In order to understand the behavior of the models when assuming that the fictitious interface may display absorption, a number of tests were performed. A response was computed for the parallelepipedic space, assigning the surface impedance of the rockwool (which was previously measured in an experimental setup which makes use of an impedance tube, meaning that impedance varies with frequency) to the discretized interface. The response provided by the MFS was compared with that obtained using BEM assuming the same properties of the rockwool. Figure 6 displays the results computed using BEM – Model 2 and MFS - Model 2. Here a relation R=5 was defined for the BEM - Model 2 and relations of R=3 and D=1.5 were set for the MFS - Model 2. The results show an excellent agreement. Note that similar results were obtained when using both BEM-

Model 1 and MFS – Model 1 (not displayed).

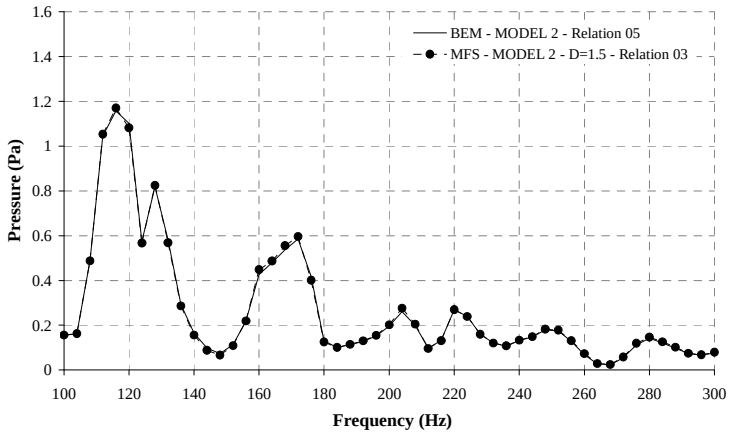

Figure 6: Pressure response obtained using the BEM – Model 2 and MFS – Model 2, assuming Robin condition in the discretized interface.

In many practical applications in building acoustics it may be required to apply different surface impedance properties to a specific interface, namely when materials with different absorption properties are applied in the same wall. The models were therefore used to compute an example of this case, assigning the surface impedance properties of two different materials to the discretized interface (by assuming that these materials are applied with the same surface area) and the responses computed again using all numerical models. The MFS – Model 2 and BEM – Model 2 results are displayed in Figure 7. The displayed results were computing setting a relation R=5 the BEM - Model 2 and relations of R=3 and D=1.5 to the MFS - Model 2. Again a good agreement between solutions was achieved. Similar results were also obtained when using both BEM - Model 1 and MFS - Model 1. The responses allow the conclusion that all models are suitable for modeling rooms with a surface displaying absorption.

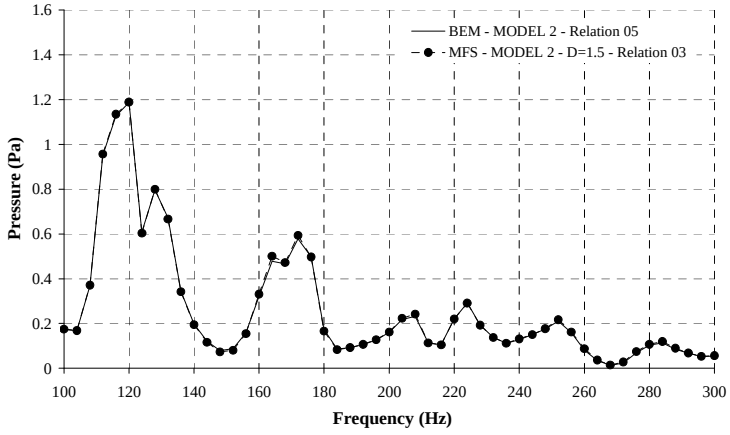

Figure 7: Pressure response obtained using the BEM – Model 2 and MFS – Model 2, assuming Robin condition in the discretized interface.

In order to assess the accuracy of the models the relative error was computed for increasing number of boundary elements/fictitious sources. Figure 8 displays these results obtained when computing the response at the above mentioned receiver position for a frequency f=100Hz, using the four models. From the analysis of this plot we find that, as expected, when

increasing the discretization or number of fictitious sources and collocation points the accuracy of the response increases. Moreover, above a 50 collocation points the MFS provides a better accuracy in relation to the BEM. We may also observe that the models which require less discretization (BEM – Model 2 and MFS – Model 2) provide a more accurate response.

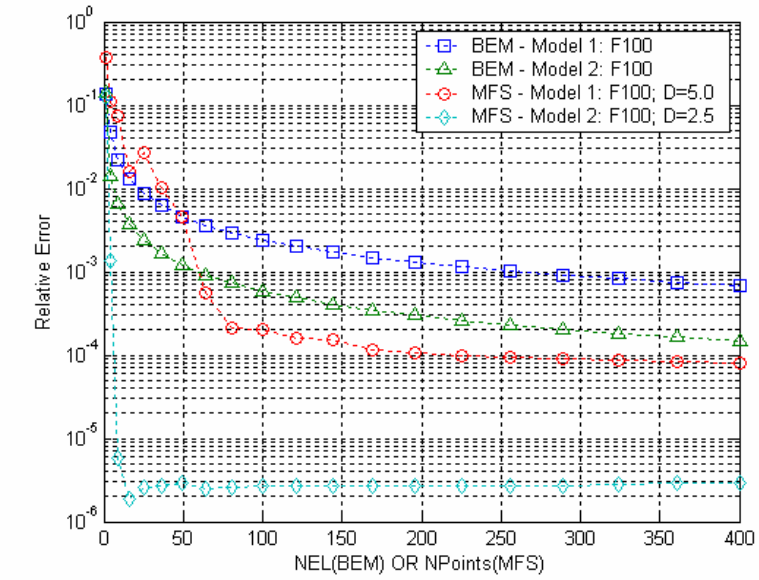

Figure 8: Relative error provided by the MFS and BEM models for a frequency of 100 Hz.

In order to analyze the performance of the models concerning to computational effort, the computation time provided by the models was obtained for a frequency of 100 Hz. The responses were computed in a computer with an AMD Turion (tm) 64 mobile technology ML-34 processor, with a clock frequency of 1.79GHz, and 1 GB of RAM. To ensure comparable results, those computation times were performed for a similar relative error of 10^{-3}. Following this demand in BEM - Model 1 and BEM – Model 2, 256 and 49 boundary elements per interface were assumed, respectively. In the MFS models this requirement is obtained assuming 64 collocation points per interface in MFS - Model 1 and 4 collocation points per interface in the MFS – Model 2. Table 1 displays the corresponding results.

Models	NEL (BEM) or NPoints (MFS) per interface	Computation time (s)
BEM – Model 1	256	125.89
BEM – Model 2	49	7123.78
MFS – Model 1	64	0.34
MFS – Model 2	4	5.23

Table 1: Computation time for a frequency f=100 Hz

The analysis of this table allows to conclude that the MFS models require less computational effort than the BEM ones, as the formulation is also more simple and does not require computation of integration schemes. When comparing BEM Model 1 with BEM Model 2 computation times we find that BEM –Model 2 is more time consuming even when much less elements are required. In fact, the Green's function used in BEM - Model 2, which is given by expression (10), requires a significant number of terms to attain convergence

leading to higher computation times. The same feature may be observed in the MFS - Model 1 and MFS – Model 2 efficiency.

The stability of the MFS with regards to the position of the fictitious sources was assessed by computing the pressure at receiver (0.4m, 0.4m, 0.5m), for frequencies between 100 Hz and 300 Hz, using the analytical solution and the MFS - Model 2 for varying relations (D) between the distance of the fictitious sources to the boundaries and the distance between collocation points. As for the relation R, in MFS – Model 1 a fixed relation of R=12 was assumed, and in MFS – Model 2 a relation R=2 was set.

Figure 9 plots the responses obtained for several distances D. In these plots it is possible to observe that when using MFS - Model 1 (see Figure 2a), for a small relation (D=0.5) the MFS does not provide an accurate response. However as the relation (D) increases the responses predicted by the MFS approach the analytical one, denoting that the model tends to display a stable behavior for increasing distances. When looking to the responses predicted by the MFS – Model 2 (see Figure 2b), again it is possible to observe that for a lower relation D, the model is not providing a proper response. For increasing relations the MFS displays a good agreement with the analytical response, however in a limited range of relations D. In fact, for a relation D=10, the MFS displays discrepancies in relation to the analytical solution, mainly in the lower frequencies.

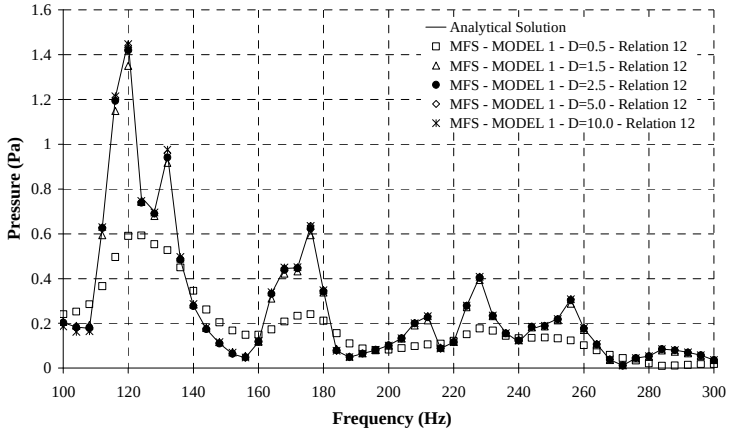

a)

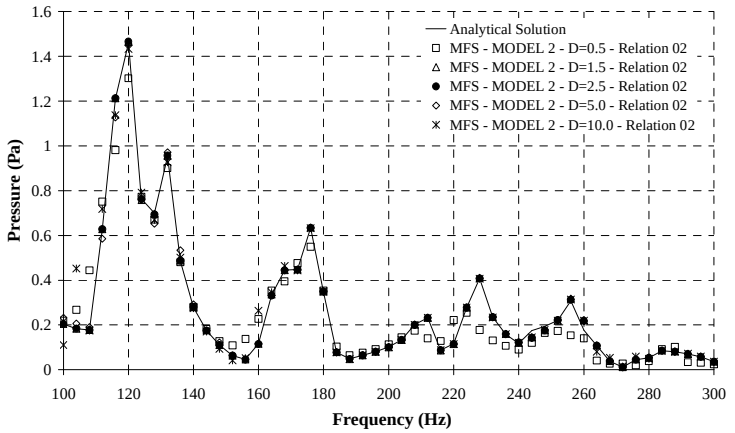

b)

Figure 9: Pressure response obtained using the analytical solution, MFS – Model 1 (a) and MFS – Model 2 (b) for varying relations (D) between the distance of the fictitious sources to the interface and the distance between collocation points.

5 NUMERICAL RESULT VS. EXPERIMENTAL RESULT

Taking into account the results obtained in the previous section, the MFS - Model 2 was used to compute the low frequency sound pressure field obtained inside a small room with dimensions 1.3mx1.4mx1.5m which corresponds to a reduced size acoustic chamber that exists in the Department of Civil Engineering of the University of Coimbra (picture of this chamber is displayed in Figure 10). In one of its faces, a 0.5x0.5 m^2 opening is inserted, allowing access to its interior. Experimental tests were also performed to obtain the pressure field in this chamber and the results were compared with predictions. Inside this chamber, a dodecahedrical sound source (B&K Omni Power 4292) has been placed, 0.40m from its front wall, and 0.40 m from its right side wall; sound levels were registered at a microphone (type 40AF from Gras Sound & Vibration), located at a symmetrical position with relation to the source, and 0.5 m above the floor. Time responses were acquired using a dBBati32 system, from 01dB, and then transformed to the frequency domain by means of FFT.

This system has also been modeled numerically, making use of the above described MFS – Model 2, considering all surfaces to be rigid. These results are displayed in Figure 11, together with marks at the positions of predicted normal modes for an exact paralellepipedic rigid chamber. These modes may be estimated using the following expression (L. Beranek, 1960):

$$f_{n,m,k} = \frac{c}{2}\sqrt{\frac{n^2}{L_x^{\,2}} + \frac{m^2}{L_y^{\,2}} + \frac{k^2}{L_z^{\,2}}}\ , \text{(Hz)} \tag{11}$$

where n, m and k are the order number of the eigenmodes along three orthogonal directions (x, y and z), L_x, L_y and L_z are the dimensions of the acoustic space along the same directions and c is the speed of sound.

Figure 10: Picture of the test chamber.

Comparing the curves of Figure 11, it is clear that they follow very similar trends, in spite of visible amplitude differences. It is important to note that the numerical result has been computed considering rigid surfaces, while in the experimental model a small amount of acoustic absorption exists, influencing the results. More importantly, the peak positions of the two curves match, in general, very well, and also correspond to the analytical normal modes prediction. However, the peak occurring at 220 Hz in the experimental result is not so well reproduced by the numerical results, and appears slightly shifted to the right. It is important to note that the difference is even larger for the analytical solution, indicating that the presence of the irregularity and of a plate in the front wall may be introducing some modifications in the dynamic behavior.

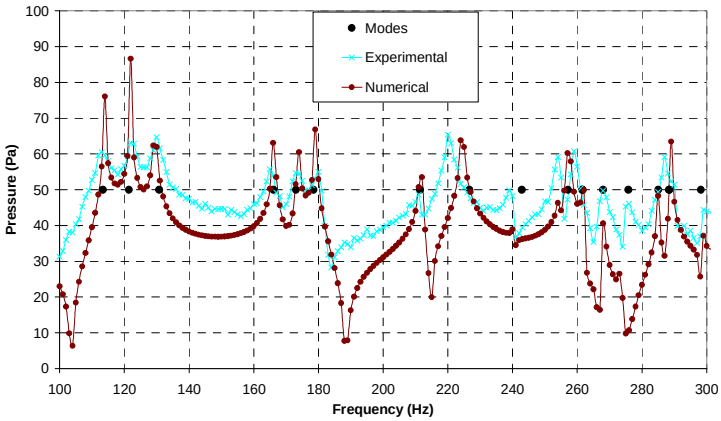

Figure 11: Pressure field provided by numerical model and by experimental tests.

6 CONCLUSIONS

This paper has addressed the use of frequency domain formulations using the Boundary Element Method and the Method of Fundamental Solution in the prediction of the three dimensional sound pressure field generated inside a parallelepiped space. The proposed formulations make use of Green's functions that allow to avoid the discretization of parts of the domain. The advantages of using this procedure have been investigated. The performed analysis allowed the conclusion that all numerical formulations are suitable in the analysis of the physical problem. The proposed models allowed to adequate compute the sound field assuming more generic geometries. It was possible to conclude that good results were obtained when assuming perfectly rigid spaces but also when assigning absorption to some of the interfaces.

When using the MFS approach the analysis allowed further conclusion that accuracy increases in relation to the BEM approach. Moreover, the models that require less discretization provide also better accuracy. As for efficiency the MFS models were found to be more efficient than the BEM ones, although the MFS model that requires less discretization of the domain displayed greater computation times. This behavior was found to be due to convergence of the Green's function used. The stability of the MFS with regards to the position of source points allowed the conclusion that the models are stable in a limited range of positions of source points, meaning that a primary analysis of source position is required when computing a sound pressure field problem.

Finally the MFS was used to compute the low frequency sound pressure field inside a reduced size acoustic chamber that exists in the Department of Civil Engineering of the University of Coimbra and the results were compared with experimental measurements. The obtained results allowed to observe a reasonable agreement between results.

ACKNOWLEDGEMENTS

The financial support by FCT (Fundação para a Ciência e Tecnologia) and CAPES (Coordenação de Aperfeiçoamento de Pessoal de Nivel Superior), within the scope of the FCT-CAPES convenium, is greatly acknowledged.

REFERENCES

Alves, CJS, Valtchev, SS. Numerical comparison of two meshfree methods for acoustic wave scattering, *Eng Analysis with Boundary Elements*, 29:371–82, 2005.

Antonio, J., Tadeu, A., Godinho, L., A three-dimensional acoustics model using the method of fundamental solutions, *Engineering Analysis with Boundary Elements*, 32: 6, 525-531, 2008.

Beranek, L., *Noise Reduction*, MacGraw-Hill, New York, (1960).

Brebbia, C. A., *The Boundary Element Method for Engineers*. Pentech Press, London, 1984.

Wu T. (Ed.), *Boundary element acoustics*, WIT Press, Southampton, UK, 2000.

Chen, JT, Chang, MH, Chen, KH, Chen, IL. Boundary collocation method for acoustic eigenanalysis of three-dimensional cavities using radial basis function. *Comput Mech*, 29: 392–408, 2002.

Fairweather, G, Karageorghis, A, Martin, PA. The method of fundamental solutions for scattering and radiation problems, *Eng Analysis with Boundary Elements*, 27:759–69, 2003.

Godinho, L., António, J., Tadeu, A., 3D sound scattering by rigid barriers in the vicinity of tall buildings, *Applied Acoustics*, 62: 11, 1229-1248, 2001.

Lacerda, LA., Wrobel, LC., Mansur, WJ., A dual boundary element formulation for sound propagation around barriers over an infinite plane, *Journal of Sound and Vibration*, 202, 235–347, 1997.

Lacerda, LA., Wrobel, LC., Power, H., Mansur, WJ., A novel boundary integral formulation for three-dimensional analysis of thin acoustic barriers over an impedance plane, *Journal of the Acoustical Society of America*, 104(2), 671–8, 1998.

Tadeu, A., António, J., Amado Mendes, P., Godinho, L., Sound pressure level attenuation provided by thin rigid screens coupled to tall buildings, *Journal of Sound and Vibration*, 304: 3-5, 479-496, 2007.